Micelles of Diblock Copolymers with Charged and Neutral Blocks: Scaling and Mean-Field Lattice Approaches

ARTICLE *in* MACROMOLECULES · APRIL 2000

Impact Factor: 5.8 · DOI: 10.1021/ma9917491

3 AUTHORS, INCLUDING:

Nadya Shusharina
Massachusetts General Hospital
39 PUBLICATIONS **453** CITATIONS

SEE PROFILE

Micelles of Diblock Copolymers with Charged and Neutral Blocks: Scaling and Mean-Field Lattice Approaches

Nadezhda P. Shusharina,*,† Per Linse,† and Alexei R. Khokhlov‡

Physical Chemistry 1, Center for Chemistry, and Chemical Engineering, Lund University, P.O. Box 124, S-221 00 Lund, Sweden; and Physics Department, Moscow State University, 117234 Moscow, Russia

Received October 19, 1999; Revised Manuscript Received February 14, 2000

ABSTRACT: Polymer micelles composed of block copolymers with one charged and one neutral block in aqueous salt free solution are analyzed by scaling and mean-field lattice theory. We study the micellar structure as a function of the length of the both blocks and the fractional charge of the hydrophilic block. The diagram of the different regimes of the behavior of the equilibrium micellar sizes is constructed. The distribution of the counterions in the system is examined using the scaling and the mean-field approaches. The numerical mean-field results are found to be consistent with three scaling regimes: a quasineutral at small fractional charge, the "Pincus" regime where the Coulomb interaction in the corona is unscreened since the counterions are located outside the corona region, and an osmotic regime where the Coulomb interactions are screened by counterions located in the corona region.

1. Introduction

Recently, intensive attention has been paid to the studies of micelles of block copolymers formed in dilute solution in a selective solvent. One of the most interesting cases is connected with aqueous solutions of block copolymers with one hydrophobic and one charged water-soluble block. When these polymers self-assemble, the hydrophobic blocks form the core of the micelle, while the charged blocks constitute the micellar corona. Several examples of experimental investigation of such systems can be found in refs 1−7.

Different theoretical approaches are available to study these systems. Scaling theory has given fundamental knowledge of polymer systems.[8,9] In the framework of the scaling approach, polyelectrolyte solutions[10,11] and neutral spherical micelles[12] have been analyzed. Subsequently, properties of micelles formed by diblock copolymers with neutral and charged blocks in solutions have been investigated.[13−17]

Mean-field theories constitute another powerful technique to examine polymer systems. A lattice version of a mean-field theory was developed by Scheutjens and Fleer[18−20] for the adsorption of homopolymers from a binary mixture. The application of this theory to micellar systems was done by Leermakers and Scheutjens[21,22] for surfactant systems and then applied to polymer micelles.[23,24] This approach was successfully used for the modeling of poly(ethylene oxide)−poly(propylene oxide) (PEO−PPO) nonionic systems.[25−27] The mean-field lattice theory initially developed for noncharged polymers was later extended to polyelectrolytes.[28,29] Mean-field lattice theory for the adsorption of weakly charged polyelectrolytes at planar and oppositely charged surface has been applied during recent years.[30−32] It is therefore tempting to apply this approach for describing micelles formed by block copolymers with one charged block.

In the present paper we will give a more extended scaling description of charged polymer micelles. Throughout, we will discriminate between regimes where the counterions are predominantly either within or outside the brush formed by the charged blocks. In particular, we have identified a so-called "Pincus" regime and moreover improved the description of the osmotic regime previously described.[16] In addition, we will compare predictions of the scaling approach with results from the mean-field lattice theory. Both methods have their advantages and disadvantages. The scaling method allows a full determination of regimes with different behavior. However, it is only possible to determine power law dependencies of the main characteristics of the micellar structure. On the other hand, the mean-field lattice method gives numerical predictions of the system behavior at given set of parameters, including the crossover regimes, but it is not so easy to obtain the full picture of possible regimes. Therefore, the combinations of these two methods gives a much more detailed understanding of the main physical effects of the system under consideration, as previously was demonstrated for polyelectrolyte brushes.[34]

2. Model

The scaling and mean-field lattice theory will be applied on, as far as possible, a common model representing a solution of a diblock copolymer. Block A consists of N_A charged monomers and block B of N_B neutral ones, and the solvent is good for the A block but poor for the B block. Both blocks are supposed to be geometrically identical and flexible; characteristic monomer volume $v \sim a^3$, where a is the linear size of a monomer. We suppose that the polymer chains are dissolved in polar medium (e.g., in water) with a uniform dielectric permittivity ϵ at temperature T and that each A block gains τN_A elementary charges, τ being the fraction of univalently charged monomers. In both the scaling and mean-field models, we however assign the fractional charge $-\tau|e|$ to each A monomer, where $|e|$ is the charge of an electron and where τ now will be referred to as the fractional charge of each A monomer. For simplicity we also suppose that the low-molecular-

† Lund University.
‡ Moscow State University.

10.1021/ma9917491 CCC: $19.00
Published on Web 04/29/2000

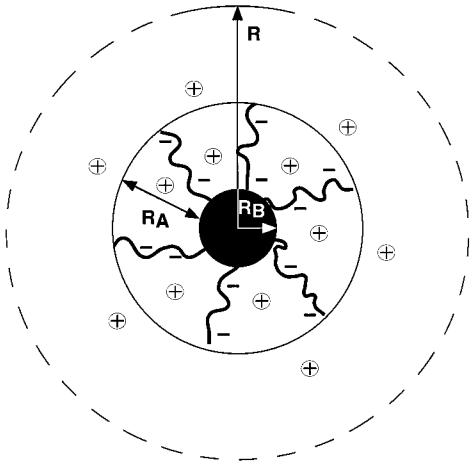

Figure 1. Schematic representation of one cell containing one block copolymer micelle. R is the radius of the cell, R_A the width of the corona formed by the charged monomers, and R_B the radius of the neutral core formed by neutral monomers.

weight ions present in the solution are counterions of valency $z = 1$.

We assume throughout that the polymer concentration is higher than the critical micelle concentration, and hence polymer micelles are always present. We divide the solution into hypothetical, identical, and spherical cells (subsystems) of radius R. Each cell contains one micelle formed by m block copolymers and its accompanying solution. The radius of the micelle is $R_M = R_A + R_B$, where R_A is the width of the corona and R_B the radius of the core (see Figure 1). We will also suppose that the half of the average distance between the centers of nearest neighboring micelles in the solution R is larger than the radius of the micelle R_M, so the micelles do not overlap. Below we will focus on the micellar aggregation number m and the sizes R_A and R_B at equilibrium.

3. Scaling Theory

We will present a more extended scaling theory for an individual micelle made of diblock copolymers with one charged block dissolved in a extremely selective solvent without added low molecular weight salt. The whole region of possible values of the system parameters is examined, and the distribution of counterions in the system is investigated thoroughly. As commonly practiced, we will omit numerical coefficients in most of the formulas below.

3.1. Basic Assumptions. Since we assume the solvent to be extremely poor for the B blocks, we regard the B blocks as collapsed and that there is practically no solvent inside the micellar core. Therefore, the volume fraction of the B monomers in the collapsed state is essentially unity and, thus

$$R_B \sim N_B^{1/3} m^{1/3} a \tag{1}$$

The soluble A blocks may by considered as end-grafted chains with grafting density

$$1/\sigma \sim m/R_B^2 \sim \frac{m^{1/3}}{N_B^{2/3} a^2} \tag{2}$$

where eq 1 has been used. Moreover, we will consider only the case of weakly charged A blocks so that the fractional charge of the A monomers is limited by the condition $\tau \ll 1$.

To find the structural characteristics of a micelle at equilibrium one should minimize the free energy of one cell counted per chain with respect to m. In the following, the free energy and the results for different regimes are presented.

3.2. Free Energy. The free energy of one cell can be written as a sum of three contributions (cf. ref 12)

$$\frac{F}{k_B T} = \frac{F_{core}}{k_B T} + \frac{F_{surf}}{k_B T} + \frac{F_{corona}}{k_B T} \tag{3}$$

where k_B is the Boltzmann constant. The first term in eq 3 is the free energy of the core made of B blocks:

$$\frac{F_{core}}{k_B T} \sim \frac{R_B^2}{N_B a^2} \sim \frac{m^{2/3}}{N_B^{1/3}} \tag{4}$$

In the scaling language this term is the stretching energy of the B blocks from the Gaussian size $N_B^{1/2} a$ to the size R_B. The second term in eq 3 is the surface free energy

$$\frac{F_{surf}}{k_B T} \sim \gamma \frac{R_B^2}{m} \sim \gamma a^2 \frac{N_B^{2/3}}{m^{1/3}} \tag{5}$$

where $\gamma \equiv \kappa/k_B T$ with κ being the interfacial tension between completely collapsed B blocks and the solvent (or solution of A monomers). The third term in eq 3 is the free energy of the corona including the contribution from the counterions. We will use known scaling results from the theory of polymer brushes[37−41] to derive F_{corona}. Depending on the relative block length, three main cases of the corona geometry will be considered: individual grafted polyions, planar brush, and spherical brush.

3.3. Individual Grafted Polyions. If the A blocks are short in comparison with the B blocks and the grafting density $1/\sigma$ is sufficiently low, the individual A blocks of the corona do not interfere with each other and they can be thought as individual chains sewed to a planar surface, and we have the so-called mushroom structure (see refs 12 and 16).

In the case of neutral A blocks, the thickness of the corona is equal to the size of an individual polymeric coil in good solvent according to

$$R_A \sim N_A^{3/5} a \tag{6}$$

If a A block is charged, two dominating forces affect its extension: a Coulomb force which tends to stretch it and a elastic force opposing the stretching. In a salt-free and sufficiently diluted solution, the block loses its counterions and the charged groups on the chain interact via an unscreened Coulomb repulsive force (cf. ref 35)

$$\frac{f_{Col}}{k_B T} = \frac{Q^2}{\epsilon k_B T R_A^2} = \frac{N_A^2 \tau^2 l_B}{R_A^2} \tag{7}$$

where $Q = N_A \tau e$ is the total charge of a A block and $l_B = e^2/\epsilon k_B T$ the Bjerrum length. The elastic force is related to conformational entropy losses in the stretched chain

(cf. refs 42 and 35 for the case of good solvent):

$$\frac{f_{conf}}{k_B T} \sim \frac{R_A^{3/2}}{N_A^{3/2} a^{5/2}} \tag{8}$$

When these forces balance each other, the thickness of the corona is given by

$$R_A \sim N_A \tau^{4/7} u^{2/7} a \tag{9}$$

where $u \equiv a/l_B$.

The conformation of a charged grafted macromolecule which is affected by Coulomb interactions may be thought as a sequence of "stretching" electrostatic blobs.[8] The size of the blob in good solvent is[35]

$$\xi_{el} \sim k_B T / f_{Col} \sim \tau^{-6/7} u^{-3/7} a \tag{10}$$

3.4. Planar Brush. If the A blocks still are short in comparison with the B blocks, but the grafting density $1/\sigma$ is higher, the A blocks are sewed to a surface which can be regarded as flat and we have the case of a planar brush.

Below we will repeat the general results of ref 12 for the micelles with neutral A blocks to guide the reader successively through the theoretical consideration. In the Alexander−de Gennes brush model language,[43] the concentration of monomers within the brush is constant. The free energy of the outer layer of the corona is then of the order of the number of "concentration" blobs in a grafted chain in $k_B T$ units.[8] The blob size $\xi_{conc} \sim g^{3/5} a$, where g is the number of monomers within the blob, the width of the brush R_A, and the free energy of the outer layer of the micelle per chain for this case are given by (cf. refs 12 and 37)

$$\xi_{conc} \sim \sigma^{1/2} \sim \frac{N_B^{1/3}}{m^{1/6}} a \tag{11}$$

$$R_A \sim \frac{N_A}{g} \xi_{conc} \sim \frac{N_A}{N_B^{2/9}} m^{1/9} a \sim R_B \Omega \tag{12}$$

$$\frac{F_{conc}}{k_B T} \sim \frac{N_A}{g} \sim \frac{R_A^{5/2}}{N_A^{3/2} a^{5/2}} \sim \frac{N_A}{N_B^{5/9}} m^{5/18} = m^{1/2} \Omega \tag{13}$$

where

$$\Omega \equiv \frac{N_A}{m^{2/9} N_B^{5/9}} \tag{14}$$

In the case of individual grafted coils (see previous section), $g = N_A$, and hence

$$\frac{F_{conc}}{k_B T} \sim 1 \tag{15}$$

Regarding charged A blocks, the contribution to the free energy from the electrostatic interactions is more diverse as compared to individual grafted chains, e.g., the planar polyelectrolyte layer can hold the counterions near it. Following ref 35, let us introduce the characteristic thickness of the counterion cloud (cf. ref 44):

$$\lambda \cong l_B^{-1} \sigma e / Q \sim \frac{N_B^{2/3}}{N_A \tau} u^{-1} m^{-1/3} a \tag{16}$$

We notice that the counterions cloud thickness λ increases with decreasing fractional charge τ of the A monomers.

If $\lambda \ll R_A$, most of the counterions are located inside the corona compensating the charge of the layer. The resulting stretched force arising from the electrostatic interactions dominates by the osmotic pressure of the counterions inside the corona (referred to as the osmotic regime):[35]

$$\frac{f_{osm}}{k_B T} \sim \frac{Q}{R_A e} \sim \frac{N_A \tau}{R_A} \tag{17}$$

The equilibrium thickness of the corona can be determined from the balance of the elastic force and the electrostatic force. With the use of eqs 8 and 17, we get

$$R_A \sim N_A \tau^{2/5} a \tag{18}$$

The free energy of the corona can be written as

$$\frac{F_{corona}}{k_B T} = \frac{F_{conc}}{k_B T} + \frac{F_{osm}}{k_B T} \sim \frac{N_A}{N_B^{5/9}} m^{5/18} + N_A \tau \ln m \tag{19}$$

where eqs 13 and 17 have been employed. In the osmotic regime, each grafted A block may be regarded as a sequence of stretched electrostatic blobs of size

$$\xi_{el} \sim k_B T / f_{osm} \sim \tau^{-3/5} a \tag{20}$$

When $\lambda \gg R_A$, most of the counterions are outside the micellar corona, and an electrical double layer is formed outside the core (referred to as the Pincus regime). The mean electrostatic force per A block acting in the direction perpendicular to the core surface is proportional to surface charge density:[35]

$$\frac{f_{Col}}{k_B T} \sim \frac{Q^2}{\epsilon k_B T \sigma} \sim \frac{N_A^2 \tau^2}{N_B^{2/3}} u m^{1/3} a^{-1} \tag{21}$$

The width of the corona R_A is determined from the balance of chain elasticity and this stretching electrostatic force. With the use of eqs 8 and 21, we have

$$R_A \sim \frac{N_A^{7/3} \tau^{4/3}}{N_B^{4/9}} u^{2/3} m^{2/9} a \tag{22}$$

The free energy of the corona per chain in this regime depends on an aggregation number according to the power law

$$\frac{F_{corona}}{k_B T} = \frac{F_{conc}}{k_B T} + \frac{F_{Col}}{k_B T} \sim \frac{N_A}{N_B^{5/9}} m^{5/18} + \frac{N_A^{13/3} \tau^{10/3}}{N_B^{10/9}} u^{5/3} m^{5/9} \tag{23}$$

where eqs 13 and 21 have been used. The size of stretching electrostatic blob in this case is given by

$$\xi_{el} \sim k_B T / f_{Col} \sim \frac{N_B^{2/3}}{N_A^2 \tau^2} u^{-1} m^{-1/3} a \tag{24}$$

Let us now consider the regimes where the electrostatic interactions are unimportant. With decreasing fractional charge of the A monomers, the volume intermolecular interactions begin to dominate. In the framework of the blob picture, the crossover between a "quasineutral" regime and the regime where electrostatic interactions are important is reached when the size of the concentration blob given by eq 11 becomes equal to the size of the electrostatic blob given by eq 20 or eq 24. In the "quasineutral" regime the structure of the corona is the same as for the case of neutral micelles (see ref 12).

3.5. Spherical Brush. When the corona size R_A becomes larger than the radius of the core R_B, the curvature of the corona becomes apparent. We refer this to a spherically curved brush.

For neutral A blocks, the size of the blob increases with radial coordinate r in accordance with the simplest geometric picture (see refs 12 and 37):

$$\frac{\xi_{conc}(r)}{\xi_{conc}(R_B)} \sim \frac{r}{R_B}; \quad \xi_{conc}(r) \sim g^{3/5}(r)a \tag{25}$$

The extension of the corona and the free energy becomes

$$R_A \sim N_A{}^{3/5} m^{1/5} a \simeq R_B \Omega^{3/5} \tag{26}$$

$$\frac{F_{conc}}{k_B T} \sim m^{1/2} \ln\left(\frac{N_A}{N_B{}^{5/9} m^{2/9}}\right) \simeq m^{1/2} \ln \Omega \tag{27}$$

where Ω was given by eq 14.

In the case of charged A blocks, the contribution from the electrostatic free energy becomes more elaborated. We start by applying the cell model as described in section II and by Figure 1. Moreover, we assume that there is a distribution of the counterions being inside and outside the micelle. Therefore, the total electrostatic free energy of a system "charged spherical micelle plus counterions" is given by

$$F_{el} = \frac{Q_M{}^2 \alpha^2}{\epsilon R_M} + k_B T \frac{Q_M}{e}(1-\alpha) \times \ln\left(\frac{Q_M}{e}\frac{(1-\alpha)}{R_M{}^3}\right) + k_B T \frac{Q_M}{e}\alpha \ln\left(\frac{Q_M}{e}\frac{\alpha}{R^3}\right) \tag{28}$$

where the first term is the electrostatic energy of a charged sphere of radius $R_M = R_A + R_B$ with $Q_M = mN_A\tau e$ and the next two terms denote the mixing entropy of the counterions located inside and outside the micelle, respectively, with α denoting the fraction of the counterions outside the micelle.

To obtain the equilibrium distribution of the counterions, F_{el} should be minimized with respect to α. This leads to the following equation:

$$\frac{Q_M{}^2 \alpha}{\epsilon R_M} + k_B T \frac{Q_M}{e} \ln\left(\frac{\alpha}{1-\alpha}\frac{R_M{}^3}{R^3}\right) = 0 \tag{29}$$

From eq 29 the following expressions for α can be obtained:

$$\alpha = \begin{cases} \frac{1}{z}\ln\frac{1}{\Phi_{mic}} & \text{if } \alpha \ll 1, \\ 1 - \Phi_{mic} e^z & \text{if } 1-\alpha \ll 1 \end{cases} \tag{30}$$

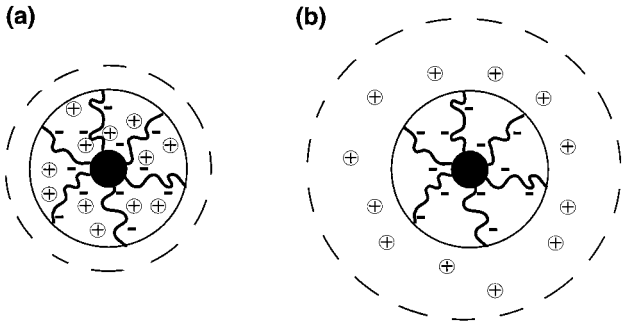

Figure 2. Illustration of two concentration ranges of the micellar solution: (a) $\Phi_{mic} > e^{-z}$ (see text for definition of Φ_{mic} and z) where the counterions are inside the corona of the micelle and (b) $\Phi_{mic} < e^{-z}$ where the counterions are outside the corona and in the intermicellar solution.

$$z \equiv \frac{Q_M}{e}\frac{l_B}{R_M} \tag{31}$$

Here $\Phi_{mic} \equiv R_M{}^3/R^3$ is a volume fraction of the micelles in the solution. A physical interpretation of the parameter z is the electrostatic interaction energy between the charged micelle and a counterion located on the perephery of the corona (specifically at the distance R_M from the center of the micelle) divided by the thermal energy. If $z \gg 1$, the electrostatic interactions dominate and the counterions are associated the micelle, whereas in the opposite case, $z \ll 1$, the thermal energy prevails over the electrostatic one and the counterions are spread in the solution.

The limiting cases of eq 30 correspond to the situation where counterions are mainly present either inside the micelle or outside it. At fixed z, the crossover between these regimes is determined by the micelle volume fraction in the solution. At $\Phi_{mic} > e^{-z}$ most counterions are within the spherical corona (see Figure 2a), whereas if $\Phi_{mic} < e^{-z}$ most of the counterions are outside the micelle (see Figure 2b). Hence, there are two different concentration ranges of the micellar solution. The electrostatic contribution to the free energy of the cell per chain in each of these cases is given by the expressions (only main dependences on m are taken into account):

$$\frac{F_{el}}{k_B T} \equiv \frac{F_{el}/m}{k_B T} \sim \begin{cases} N_A \tau \ln m & \text{if } \Phi_{mic} > e^{-z}, \\ N_A \tau \ln m + N_A \tau z & \text{if } \Phi_{mic} < e^{-z} \end{cases} \tag{32}$$

The case $\Phi_{mic} > e^{-z}$ will be referred to as the osmotic regime of spherical brushes (cf. refs 36 and 41). The electrostatic force is the same as in the osmotic regime of planar brush and the equilibrium thickness of the corona is given also by eq 18. The free energy of the corona in the osmotic regime of spherical brushes can be obtained from eq 27 and the first line of eq 32:

$$\frac{F_{corona}}{k_B T} = \frac{F_{conc}}{k_B T} + \frac{F_{osm}}{k_B T} \sim m^{1/2} \ln\left(\frac{N_A}{N_B{}^{5/9} m^{2/9}}\right) + N_A \tau \ln m \tag{33}$$

If $\Phi_{mic} < e^{-z}$, the charged A monomers within the brush interact through the unscreened Coulomb potential. The equilibrium width of the corona is determined from the balance of elastic force given by eq 8 and the electrostatic force applied to each chain given by f_{Col}/

Table 1. Scaling Relations for Aggregation Number m, Corona Thickness R_A, and Core Radius R_B of Micelles Formed by Charged Diblock Copolymers

regime	label[a]	m	R_A/a	R_B/a
		$\Phi_{mic} > e^{-z}$		
individual quasineutral chains	I(i)	N_B	$N_A^{3/5}$	$N_B^{2/3}$
planar quasineutral brush(1)	I(p1)	N_B	$N_A/N_B^{1/9}$	$N_B^{2/3}$
planar quasineutral brush(2)	I(p2)	$N_B^2/N_A^{18/11}$	$N_A^{9/11}$	$N_B/N_A^{6/11}$
sperical quasineutral brush	I(s)	$N_B^{4/5}$	$N_A^{3/5}\ N_B^{4/25}$	$N_B^{3/5}$
individual Pincus chains	II(i)	N_B	$N_A\tau^{4/7}$	$N_B^{2/3}$
planar Pincus brush(1)	II(p1)	N_B	$N_A^{7/3}\tau^{4/3}/N_B^{2/9}$	$N_B^{2/3}$
planar osmotic brush(1)	III(p1)	N_B	$N_A\tau^{2/5}$	$N_B^{2/3}$
planar osmotic brush(2)	III(p2)	$N_B^2/N_A^3\tau^3$	$N_A\tau^{2/5}$	$N_B/N_A\tau$
spherical osmotic brush	III(s)	$N_B^2/N_A^3\tau^3$	$N_A\tau^{2/5}$	$N_B/N_A\tau$
		$\Phi_{mic} < e^{-z}$		
planar Pincus brush(2)	II(p2)	$N_B^2/N_A^{39/8}\tau^{15/4}$	$N_A^{5/4}\tau^{1/2}$	$N_B/N_A^{13/8}\tau^{5/4}$
spherical Pincus brush	II(s)	$N_B^{7/11}/N_A^{21/22}\tau^{15/11}$	$N_A^{8/11}\ N_B^{2/11}\tau^{2/11}$	$N_B^{18/33}/N_A^{7/22}\tau^{5/11}$

[a] Notation key: I, II, and III denote a regime with insignificant electrostatic interactions, a Pincus regime, and an osmotic regime, respectively; i, p, and s denote individually grafted polyions, planar brush, and spherical brush, respectively. Any figures appearing discriminate regimes of the same type but with different scaling properties.

$k_BT \sim N_A^2\tau^2 m l_B/R_A^2$, and the width becomes

$$R_A \sim N_A\tau^{4/7}u^{2/7}m^{2/7}a \tag{34}$$

The corona free energy is given by the sum of eq 27 and the second line of eq 32:

$$\frac{F_{corona}}{k_BT} = \frac{F_{conc}}{k_BT} + \frac{F_{Col}}{k_BT} \sim m^{1/2}\ln\left(\frac{N_A}{N_B^{5/9}m^{2/9}}\right) + N_A\tau\ln m + N_A\tau z \tag{35}$$

As one can see from eqs 33 and 35, the free energy contribution due to osmotic pressure of the counterions plays role for both concentration regimes of the micellar solution. This means that even at $\Phi_{mic} < e^{-z}$, i.e., when most of the counterions are in surrounding solution, the spherical osmotic brush regime appears at some conditions.

3.6. Diagram of States. We will now construct diagrams of possible micellar structure and scaling regimes as a function of N_A and τ. Two different diagrams will be presented corresponding to the two conditions given in eq 32.

From eq 3 and $F_{corona} = F_{conc} + F_{el}$, we can express the free energy of a cell according to

$$\frac{F}{k_BT} = \frac{F_{core}}{k_BT} + \frac{F_{surf}}{k_BT} + \frac{F_{conc}}{k_BT} + \frac{F_{el}}{k_BT} \tag{36}$$

Here the first two terms are given by eqs 4 and 5, respectively. From eqs 13, 15, and 27 we conclude that F_{conc} can be generally written as follows:

$$\frac{F_{conc}}{k_BT} \sim 1 + m^{1/2}\ln[1+\Omega] \tag{37}$$

The last term in eq 36 is the electrostatic free energy. If $\Phi_{mic} > e^{-z}$, the counterions are within the corona of the micelle (see Figure 2a). The electrostatic contribution to the free energy in this case is equal to a minimum of two contributions:

$$\frac{F_{el}}{k_BT} \sim \min\left\{N_A\tau\ln m; \frac{N_A^{13/3}\tau^{10/3}}{N_B^{10/9}}u^{5/3}m^{5/9}\right\} \tag{38}$$

If the solution of the micelles is very diluted, i.e., $\Phi_{mic} < e^{-z}$, most of the counterions are in the intermicellar region (see Figure 2b). In this case the electrostatic free energy of the micelle per chain could be written as

$$\frac{F_{el}}{k_BT} \sim \min\left\{N_A\tau\ln m; \frac{N_A^{13/3}\tau^{10/3}}{N_B^{10/9}}u^{5/3}m^{5/9}\right\} + N_A\tau^{10/7}u^{5/7}m^{5/7} \tag{39}$$

Expressions for m, R_A, and R_B at equilibrium can now be determined by a minimization of the free energy given by eq 36 with respect to m. Usually, the term F_{surf} is in competition with either of the terms F_{core}, F_{conc}, or F_{el}.

Table 1 shows the resulting scaling relations for the aggregation number m, the corona thickness R_A, and the core radius R_B of the micelle at equilibrium. To simplify the formulas, we have put $u = 1$ (at ordinary conditions in water solution: $a \sim 1$ mn, $k_BT \sim 300$ K, $\epsilon \sim 80$, and the parameter u approximately equals unity). The interfacial tension between a collapsed B blocks and the solvent corresponds to the strong segregation limit. Under this condition we are not interested in the dependence of the micellar equilibrium characteristics on the parameter γa^2, so we have omitted this dependence as well.

Figure 3 shows the diagram of different regimes of the micellar structure depending on the block length N_A and the fractional charge τ (at fixed length of the insoluble block, $N_B = \text{const}$). Figure 3a corresponds to the concentration range $\Phi_{mic} > e^{-z}$, while the diagram in Figure 3b is valid for the concentrations $\Phi_{mic} < e^{-z}$. The boundaries between the regimes in diagrams a and b in Figure 3 are given in Tables 2 and 3, respectively.

In the "quasineutral" regimes I(i), I(p1), I(p2), and I(s) the charge of the A block is of no importance, and the scaling relations are the same as for a neutral outer block (see ref 12).

In more detail, in regime I(i) the grafting density $1/\sigma$ of the A blocks is so small that the coils do not interfere with each other ($R_A < \sigma^{1/2}$) and there is only one blob in each chain $g \sim N_A$ (cf. eqs 11 and 12).

In the regime I(p1) the corona of the micelle consists of densely packed concentration blobs; however the corona is still very thin and hence the size of the micelle is determined by the terms F_{surf} and F_{core}. The crossover between regions I(i) and I(p1) takes place at the point $\sigma^{1/2} \sim N_A^{3/5}a$ or $N_A \sim N_B^{5/18}$.

Regime I(p2) is also a regime of planar geometry for the A block, but as the length of the outer block is larger than for regime I(p1), the micellar structure is now

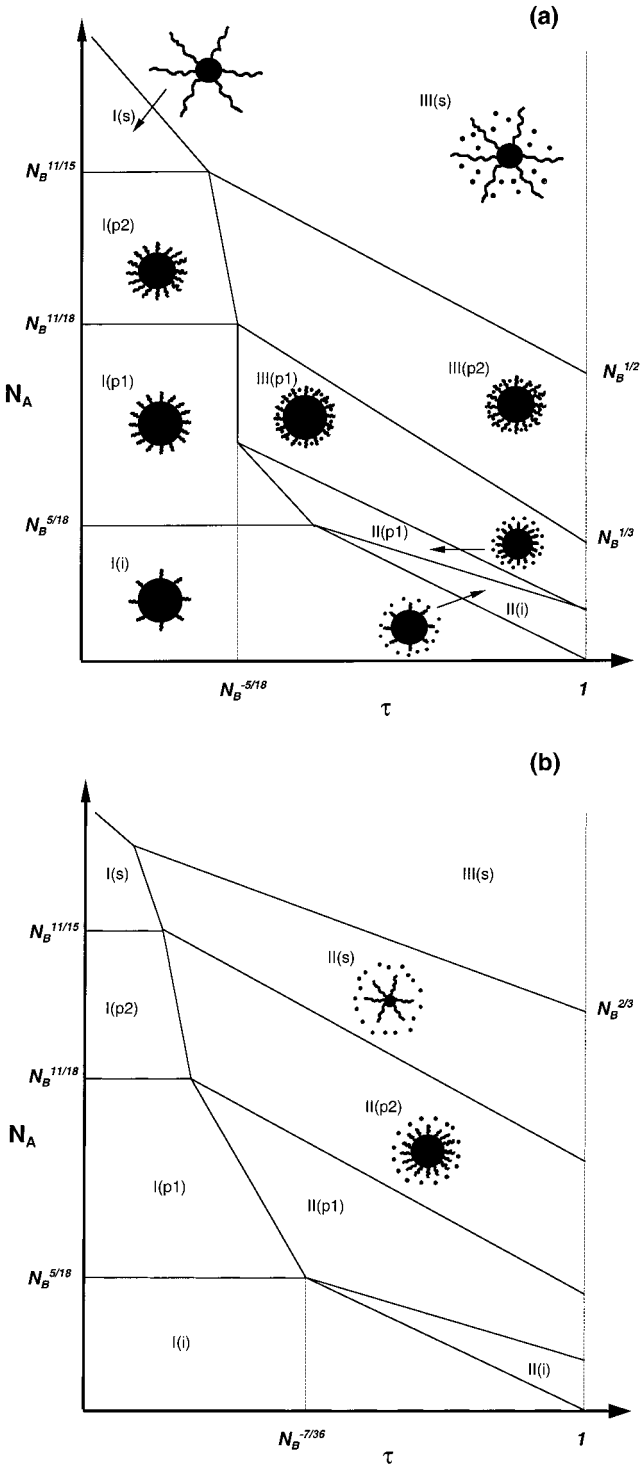

Figure 3. Diagrams displaying regimes of different micellar structure and simple illustrations of the micellar structure and the location of the counterions (dots) for (a) $\Phi_{mic} > e^{-z}$ and (b) $\Phi_{mic} < e^{-z}$ (see text and Figure 2). The equilibrium characteristics of the micelles and the key to the labeling are given in Table 1. The crossover boundaries between the regimes are presented in Tables 2 and 3.

determined by a competition of F_{surf} and F_{conc}. In this regime at fixed length of neutral block N_B, the aggregation number m and the core size R_B decrease with increasing block length N_A, whereas the corona width R_A increases (see Table 1). The equation $F_{core} = F_{conc}$ gives the crossover between the regimes I(p1) and I(p2) at $N_A \sim N_B^{11/18}$.

Table 2. Boundaries of the Regimes in the Diagram of Figure 3a

I(i)/I(p1)	$N_A \sim N_B^{5/18}$
I(p1)/I(p2)	$N_A \sim N_B^{11/18}$
I(p2)/I(s)	$N_A \sim N_B^{11/15}$
I(i)/II(i)	$N_A \sim \tau^{-10/7}$
I(p1)/II(p1)	$N_A \sim N_B^{1/12}\tau^{-1}$
I(p1)/III(p1)	$\tau \sim N_B^{-5/18}$
I(p2)/III(p2)	$N_A \sim \tau^{-11/5}$
I(s)/III(s)	$N_A \sim N_B^{2/5}\tau^{-1}$
II(i)/II(p1)	$N_A \sim N_B^{1/6}\tau^{-4/7}$
II(p1)/III(p1)	$N_A \sim N_B^{1/6}\tau^{-7/10}$
III(p1)/III(p2)	$N_A \sim N_B^{1/3}\tau^{-1}$
III(p2)/III(s)	$N_A \sim N_B^{1/2}\tau^{-7/10}$

Table 3. Boundaries of the Regimes in the Diagram of Figure 3b

I(i)/I(p1)	$N_A \sim N_B^{5/18}$
I(p1)/I(p2)	$N_A \sim N_B^{11/18}$
I(p2)/I(s)	$N_A \sim N_B^{11/15}$
I(i)/II(i)	$N_A \sim \tau^{-10/7}$
I(p1)/II(p1)	$N_A \sim N_B^{1/12}\tau^{-1}$
I(p2)/II(p2)	$N_A \sim \tau^{-22/19}$
I(s)/II(s)	$N_A \sim N_B^{-6/35}\tau^{-10/7}$
I(s)/III(s)	$N_A \sim N_B^{2/5}\tau^{-1}$
II(i)/II(p1)	$N_A \sim N_B^{1/6}\tau^{-4/7}$
II(p1)/II(p2)	$N_A \sim N_B^{8/39}\tau^{-10/13}$
II(p2)/II(s)	$N_A \sim N_B^{8/23}\tau^{-14/23}$
II(s)/III(s)	$N_A \sim N_B^{2/3}\tau^{-4/5}$

Finally, the thickness of the corona becomes of the order of radius of the core, and we enter regime I(s), where the curvature of the core surface becomes apparent. As F_{conc} specified by eq 27 depends only logarithmically on N_A, the power dependence of m and R_B on N_A disappears. From eqs 12 and 26, it follows that the crossover between the planar brush and the spherical brush regimes takes place at $N_A \sim N_B^{11/15}$ (or $\Omega \sim 1$).

Let us now describe the regimes in which the charge of the outer block is essential. Two sets of different regimes are possible depending on volume fraction of the micelles in the solution. Let us first describe the case when $\Phi_{mic} > e^{-z}$ (see Figure 2a). If the charged block is very short, so that individual grafted coils are not penetrating, the charging of the outer block leads to a stretching of each charged block in the direction perpendicular to the core surface. In this regime, II(i), the outer layer of the micelle is free of counterions and thickness of the corona is equal to length of an individual polyion in infinitely diluted salt free solution (see eq 9).

With increasing block length N_A, a layer of grafted charged chains is formed, but the total charge of this layer is not sufficient to hold the counterion inside it. This regime II(p1) corresponds to the case of planar Pincus brush. The equilibrium properties of the micelle in this regime is determined by competition between F_{surf} and F_{core}.

When the fractional charge τ or the length N_A of the outer block increases, we enter regime III. In this regime the condition $\lambda \ll R_A$ (see eq 16) is valid, so most of the counterions are inside the corona region, and we have the case of planar osmotic brush. In the regime III(p1), the characteristic parameters of the micelle are still determined by F_{surf} and F_{core}, but in the regime III(p2) the contribution to the free energy from the osmotic pressure of the counterions starts to dominate over the free energy of the core. The micellar aggregation number depends on the fractional charge of the A block in this regime (see Table 1). Finally, at even larger τ and/or N_A, the thickness of the corona R_A becomes larger than

the radius of the core R_B and we enter the spherical osmotic brush regime (regime III(s)). It should also be mentioned that the appearance of the different regions depends on the tendency of the self-association of the block copolymers. The critical micellization concentration (cmc) increases with increasing τ and N_A, but we assume that we are always above the cmc. The location of the cmc will be considered explicitly in our next publication.[46]

When $\Phi_{mic} < e^{-z}$, the spherical layer of the micelle is mostly free from counterions and only if the charged A blocks are very long the counterions are located in the corona. For this concentration region two new regimes appear (see Figure 3b). The regime II(p2) is the regime of planar Pincus brush. The equilibrium characteristics of the micelle are determined from the competition of F_{surf} and F_{el} given by the second term in the brackets of eq 39. With increasing of the length of charged block, the thickness of the corona becomes larger than the radius of the core and we have the Pincus brush of spherical curvature (regime II(s)). Note that there are no the regimes of planar osmotic brush III(p1) and III(p2) for this concentration range.

4. Mean-Field Lattice Theory

4.1. Method and Parameters. The same physical model will now be examined by employing the mean-field lattice theory. Central to the lattice theory used here is the division of the cell into concentric shells, and the division of each shell into lattice space of equal size.[25] The Bragg−Williams approximation of random mixing is applied within each layer separately, and hence all the lattice sites in a shell are equivalent. One lattice cell contains either one polymer segment, a solvent molecule, or a counterion. The model contains four different species: neutral polymer segments, charged polymer segments, counterions, and solvent.

The model involves two different types of interactions: electrostatic (charge−charge) and nonelectrostatic (the rest). The nonelectrostatic interaction between species in adjacent lattice sites is described by Flory−Huggins χ parameters. In line with random-mixing approximation, the charged species (charged polymer segments and counterions) interact with an electrostatic potential of mean force ψ_i, which depends only on layer number i. The potential of mean force is related to the charge density through Poisson's equation

$$\epsilon\nabla^2\psi_i = -4\pi\rho_i \qquad (40)$$

where ϵ is the dielectric permittivity of the medium and ρ_i is the volume charge density in layer i. In our calculations, we use an assumption of uniform dielectric permittivity. For details concerning the numerical procedure, we refer the reader to previous publications.[31−33]

The scaling results showed that the aggregation number m and the core radius R_B are independent of N_A and τ in regimes I(i), I(p1), II(i), II(p1), and III(p1); see Table 1. These regimes correspond to the situation where the radius of the micellar core is larger than the thickness of the corona (so-called "crew-cut" micelles). On the basis of this observation, a more simplified approach can be employed to examine the properties of the brush region in these regimes. In this approach, an inner hard surface, representing the core surface, was introduced in the lattice model on which charged chains were grafted with a given surface density. In the present report, we will only consider the case of fixed aggregation number and core radius and hence the more simplified model will be utilized, whereas the other cases with variable aggregation number and core radii will be considered in a separate publication.[46] Since the geometry of the micellar corona is quasiplanar, one cannot expect the transition from planar to spherical Pincus brush, and hence the results of numerical mean-field calculations will refer to the scaling diagram presented in Figure 3a.

Table 4. Parameters of the Model

quantity	value
temperature	$T = 298$ K
dielectric permittivity	$\epsilon = 80$
lattice spacing	$d = 7$ Å

For simplicity, all interaction parameters between different species and between species and surface are supposed to be zero. The temperature, dielectric constant, and lattice spacing used are collected in Table 4. In the calculations, we are specifically interested in the dependence of the thickness of the corona R_A on the length N_A of the A block and the fractional charge τ of the A block. In addition, we will also consider the distribution of the counterions in the system.

4.2. Spherical Charged Brush. In this section we present results obtained for the case of grafted charged chains. The radius of the curved grafting surface is chosen to be equal to 625 lattice layers and the grafting density $1/\sigma = 0.003185$. In comparison with experimental systems, the core radius is large, but it was nevertheless selected to be able to probe a large N_A range and still remain in a quasiplanar regime.

One of the major results of the our simplified lattice model solved by the mean-field theory is the distribution of the charged segments of the outer block and the counterions outside the micellar core. Figure 4 shows the volume fraction of the charged segments and the counterions as a function of the layer number for the fractional charge $\tau = 0.6$ at two chain lengths of the charged block. The numeration of the layers starts from the layer adjacent to the surface. In Figure 4a, we have $N_A = 150$ and nearly all the counterions are located in the brush. However, in the case of $N_A = 10$, Figure 4b shows that the majority of the counterions have escaped the brush region, since the counterion profile extends much further away from the core surface as compared to the profile of the charged segments.

In Figure 5 we present the brush thickness R_A as a function of the length of the charged block N_A at the fractional charge $\tau = 0.2$, 0.6, and 1.0. We define the brush thickness as a layer number which encompasses 90% of the total amount of the polymer segments. First, we notice that the brush thickness increases with N_A as expected. However, this increasing is dependent on τ. At sufficiently high τ, we observe a single power law dependence of R_A on N_A over the whole investigated N_A range. At the lower τ, two types of dependencies are found. In particular, at low N_A, the dependence of R_A on N_A becomes weaker. Specifically, numerical fits gave the following relations:

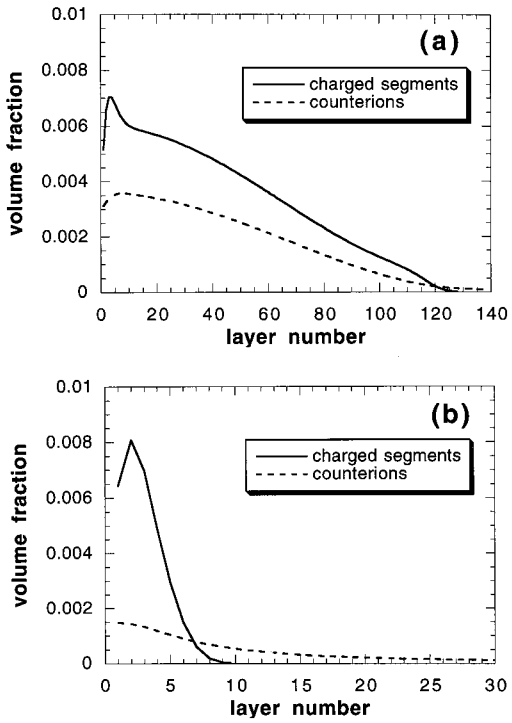

Figure 4. Volume fraction profiles of charged polymer segments and counterions vs the layer number at the fractional charge $\tau = 0.6$ and length of the charged block (a) $N_A = 150$ or (b) $N_A = 10$. Note, the different abscissa scales.

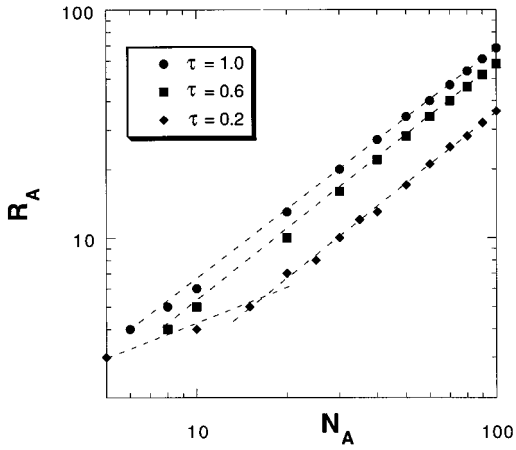

Figure 5. Brush thickness R_A vs the length N_A of the charged A block at indicated fractional charge τ shown in double logarithmic scale.

$$\tau = 1.0:\ R_A = 0.61N_A^{1.02}$$

$$\tau = 0.6:\ R_A = 0.52N_A^{1.02}$$

$$\tau = 0.2:\ R_A = \begin{cases} 1.04N_A^{0.62} & \text{for large } N_A, \\ 0.27N_A^{1.07} & \text{for small } N_A \end{cases} \quad (41)$$

Hence, if the fractional charge is high enough ($\tau =$ 1.0 or 0.6), the thickness increases with N_A according to the power law $R_A \sim N_A$. At low fractional charge ($\tau =$ 0.2) and for long A blocks the dependence on N_A is also linear, whereas if the chains are shorter the dependence becomes weaker.

Returning to the scaling analysis, we concluded that if the fractional charge is large enough, the scaling regimes I(i), II(i), II(p1), and III(p1) are expected to appear with increasing N_A (see Figure 3a). In two of them, II(i) (individual grafted polyions) and III(p1)

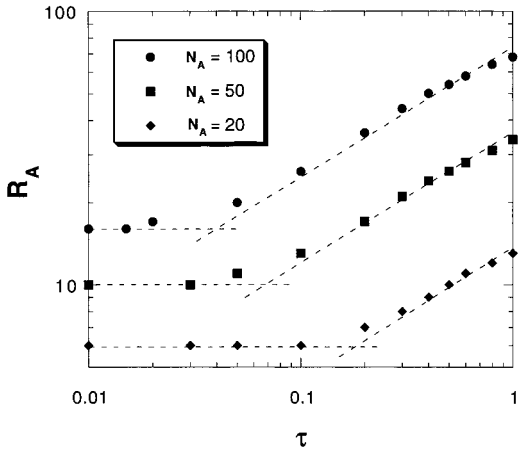

Figure 6. Brush thickness R_A vs the fractional charge τ of the A block at indicated length N_A of the charged A block shown in double logarithmic scale.

(planar osmotic brush), we have the $R_A \sim N_A$ which indeed is the scaling relation found in Figure 5 at $\tau =$ 1.0 and 0.6. Hence, we conclude that the mean-field lattice results are consistent with regimes II(i) and III-(p1). We also notice that the dependence corresponding to the regime II(p1) (the regime of planar Pincus brush) is not observed in the mean-field results. A possible reason is that this regime is too narrow to be detected.

At the lower fractional charge $\tau = 0.2$, we observed the weaker dependency $N_A^{0.62}$, which is consistent with that of regime I(i) (individual neutral coils). The change in power law dependence from $N_A^{0.62}$ to N_A at increasing τ for a given N_A would well correspond to a crossover from regime I(i) to II(i), whereas the change from $N_A^{0.62}$ to N_A at increasing N_A at fixed τ would correspond to a crossover from regime I(i) to I(p1), II(i), or III(p1). At the present state, we cannot discriminate among the regimes I(p1), II(i), and III(p1). Again, the regime II-(p1) absence could due to its narrow extension.

We have also analyzed the dependence of brush thickness on fractional charge τ of the A monomers at different chain length N_A. Figure 6 shows that at sufficiently low τ, R_A is independent of τ, whereas at larger τ, R_A increases with τ according to

$$N_A = 100:\ R_A = 71.2\tau^{0.42}$$

$$N_A = 50:\ R_A = 34.5\tau^{0.42}$$

$$N_A = 20:\ R_A = 13.1\tau^{0.40} \quad (42)$$

Hence, at low τ (e.g., $\tau < 0.07$ at $N_A = 50$), we observe the existence of a "quasineutral" regime (regimes I(i), I(p1), and/or I(p2)), whereas at high τ our data are consistent with regime III(p1). The mean-field data show that the cross over between the "quasineutral" and the "electrostatic" regimes shifts to larger τ at decreasing N_A.

We will now return to the location of the counterions. The scaling approach suggested that there exists regimes where the counterions are predominantly located inside (the osmotic regime) or outside (the Pincus regime) of the charged brush. In the lattice model, this transition is of course gradual. This is demonstrated in Figure 7, which shows the fraction of counterions located outside the brush region (referred to as free counterions), Q_{free}/Q_M, as a function of either the length of the

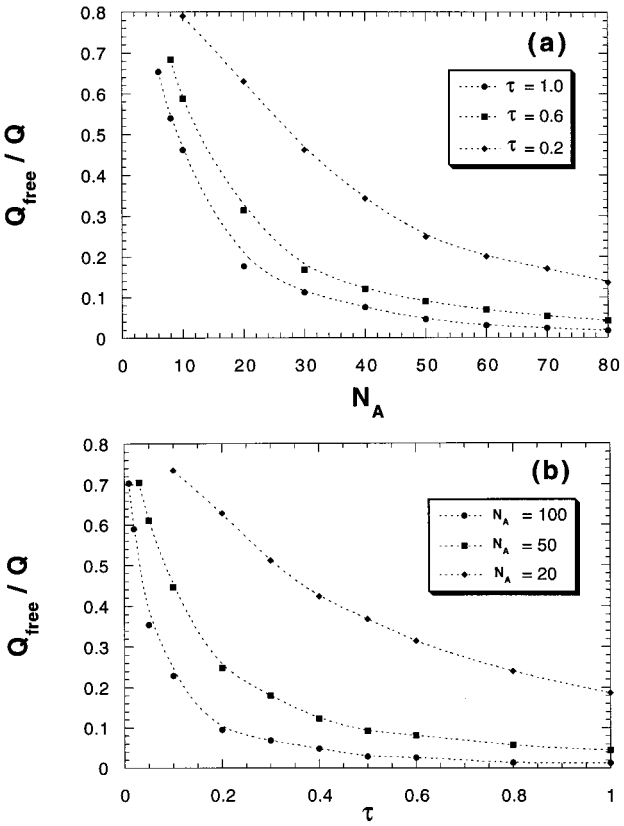

Figure 7. Fraction of free counterions Q_{free}/Q_M (see text) vs (a) the length N_A of charged A block and (b) the fractional charge τ of the A block.

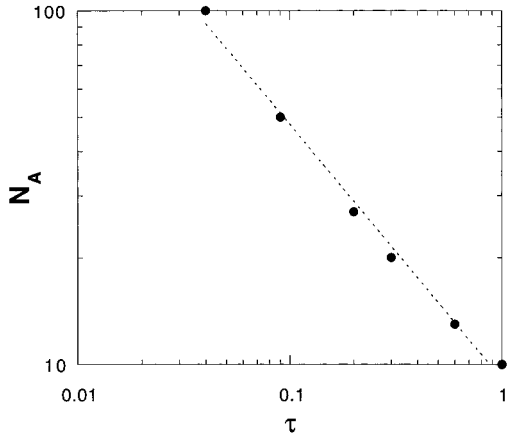

Figure 8. Crossover line which separates the two regimes of the counterions location in double logarithmic scale. Above the line, $Q_{free}/Q_M < 0.5$.

charged block N_A or the fractional charge τ of the charged segments. Here Q_{free} denotes the charge of the counterions outside the brush where the brush thickness is defined as above and $Q_M = mN_A\tau e$ with m being the number of charged chains.

Figure 7 displays the dependencies of Q_{free}/Q_M on the length N_A of the A block at different degree of fractional charge τ (Figure 7a) and on τ at different N_A (Figure 7b). Figure 7a shows that the fraction of free counterions decreases with increasing length of the A block at constant τ, whereas Figure 7b shows that the fraction of free counterions decreases at increasing fractional charge τ at fixed N_A. In other words, the grafted chains "hold" the counterions inside them if its charge is large enough, either by sufficient length or charge density.

To proceed with a comparison with the scaling theory, we define $Q_{free}/Q_M = 0.5$ as the crossover point between regimes of free and bound counterions. The crossover points obtained from the mean-field results given in Figure 7, are displayed in Figure 8 in terms of a crossover line in the (τ, N_A) space. The line in Figure 8 is described by the power dependence $N_A = 9.1\tau^{-0.72}$, which is consistent with the boundary between the scaling regimes II(p1) and III(p1) (see Table 2). The regime II(p1) is the Pincus brush regime, in which the brush is charged due to escaping of all counterions from the brush region, whereas III(p1) is the osmotic brush regime in which the charge of the brush is neutralized by the counterions which are located inside it. Hence, in this analysis we found a Pincus brush regime.

5. Discussion and Conclusions

In this paper we analyze the structure of micelles formed by charged block copolymers by using analytical scaling method and a numerical mean-field lattice model. We have constructed an extensive diagram of different regimes of the behavior of the system and presented analytical scaling relations for the micellar aggregation number, the radius of the core, and the thickness of the corona. The distribution of the counterions in the system was examined in the framework of a two-phase approximation. There are two types of diagrams according to our predictions. One corresponds to the situation when most of the counterions are inside the corona region compensating the charge of the micelle and another where only a small amount of the counterions are inside the corona.

The micellization in the solution of diblock copolymers with one charged block was previously considered theoretically.[13−16] Marko and Rabin[13] discussed the micelle formation in a solvent for two limiting cases: weakly charged corona blocks (fractional charge $\tau \ll 1$) and strongly charged corona blocks ($\tau = 1$). In a weak-charge limit, which corresponds to the case considered in the present paper, the location of the counterions inside the corona region was ignored a priory. The authors considered the case of spherical geometry of the corona and took into account Colomb repulsion of completely unscreened polyelectrolyte chains inside the corona. This regime corresponds to the Pincus spherical brush regime in our diagram. It appears if the concentration of the micelles in the solution is very low and practically is not realized in experiment. The equilibrium aggregation number and the thickness of the corona were calculated using simple scaling relations in assumption of Gaussian elasticity of the corona blocks. The same result was obtained by authors of ref 14.

Dan and Tirrel[15] applied a scaling model to describe a micellization of charged−neutral diblock copolymers in dilute salt solution. They considered strongly charged blocks assuming moderately high salt concentration. The equilibrium aggregation number and the radius of the core were found to be charge and salt independent, whereas the corona thickness decreases with salt concentration.

In our previous work,[16] the structure of polyelectrolyte micelle was considered in the framework of a scaling theory. We constructed the diagram of different scaling regimes assuming that counterions are inside the spherical corona. However, changing corona geometry from spherical to planar can lead to the situation when

counterions escape from the corona region. This case corresponds to the planar Pincus regime characterized by unscreened Colomb interactions of polymer segments inside the corona. This regime was not considered in ref 16.

The lattice modeling was here restricted to the cases of micelles with fixed aggregation number and core size. Because of the relation between the radius of grafting surface and the length of grafted chains the geometry of the corona layer was quasiplanar. This selection allowed us to obtain the dependencies of the corona thickness as a function of the length of charged chain and the fractional charge in some region of the scaling diagrams. The numerical results were in excellent agreement with the scaling relations for the quasineutral and the osmotic regimes. Moreover, the analysis of the distribution of the counterions gave us the condition for boundary between osmotic brush and Pincus brush regime. The scaling exponent of this crossover was fully recovered from the mean-field lattice modeling results.

Nevertheless, the Pincus brush regime was not detected in the scaling analysis of the corona thickness. A likely reason for this fact is that the range of the parameters in which this regime can be detected is too narrow in comparison with the ranges corresponding other neighboring regimes, so that the crossovers between these regimes cover the width of the Picus regime. We expect that due to the same reason this regime will be difficult to detect experimentally.

The obtained results show that the most important regimes for the structure of the charged corona of "crew-cut" micelle are the quasineutral regime at low fractional charge and the osmotic regime, which is characterized by the screening of the Coulomb repulsion by counterions inside the corona region, at higher fractional charge.

Unfortunately, there are still no systematic experimental investigations of the system considered in this paper. Some measurements confirm the general tendencies predicted by scaling.[4] Increasing of the insoluble block length and decreasing of the polyelectrolyte block length promote the micelle formation, whereas, the charge of the corona blocks is an unfavorable factor for the micellization. In other papers, solutions with moderately high salt concentration were considered,[5,6] since no micelles were observed in salt free solution. It should mentioned that if the solvent is extremely poor for the blocks forming the core, the micelles are frozen, especially if the glass transition temperature of the core is above the experimental temperature. Therefore, in this case the system is not in equilibrium impeding a direct comparison of experimental data with theory.

Acknowledgment. N.P.S. is grateful to O. Borisov and E. Zhulina for fruitful discussions and comments. This work was financed by the Swedish Research Council for Engineering Science (TFR) and the Swedish National Research Council (NFR).

References and Notes

(1) Wu, G.; Zhou, Z.; Chu, B. *Macromolecules* **1993**, *26*, 2117.
(2) Astafieva, I.; Zhong, X. Fu; Eisenberg, A. *Macromolecules* **1993**, *26*, 7339.
(3) Khougaz, K.; Gao, Zh.; Eisenberg, A. *Macromolecules* **1994**, *27*, 6341.
(4) Khougaz, K.; Astafieva, I.; Eisenberg, A. *Macromolecules* **1995**, *28*, 7135.
(5) Baines, F. L.; Armes, S. P.; Billingham, N. C.; Tuzar, Z. *Macromolecules* **1996**, *29*, 8151.
(6) Guenoun, P.; Davis, H. T.; Tirrell, M.; Mays, J. *Macromolecules* **1996**, *29*, 3965.
(7) Zhang, L.; Eisenberg, A. *Polym. Adv. Technol.* **1998**, *9*, 677.
(8) de Gennes, P.-G. *Scaling Concepts in Polymer Physics*; Cornell University Press: Ithaca, NY, 1979.
(9) Grosberg, A. Yu.; Khokhlov, A. R. *Statistical Physics of Macromolecules*; American Institute of Physics: New York, 1994.
(10) de Gennes, P.-G.; Pincus, P.; Velasco, R. M.; Brochard, F. *J. Phys. Fr.* **1976**, *37*, 1461.
(11) Khokhlov, A. R.; Khachaturian, K. A. *Polymer* **1982**, *23*, 1742.
(12) Zhulina, E. B.; Birshtein, T. M. *Vysokomol. Soedin. A* **1985**, *27*, 511; Birshtein, T. M.; Zhulina, E. B. *Polymer* **1989**, *30*, 170.
(13) Marko, J. F.; Rabin, Y. *Macromolecules* **1992**, *25*, 1503.
(14) Witten, J.; Joanny, J. F. *Macromolecules* **1993**, *26*, 2691.
(15) Dan, N.; Tirrell, M. *Macromolecules* **1993**, *26*, 4310.
(16) Shusharina, N. P.; Nyrkova, I. A.; Khokhlov, A. R. *Macromolecules* **1996**, *29*, 3167.
(17) Shusharina, N. P.; Saphonov, M. V.; Nyrkova, I. A.; Khalatur, P. G.; Khokhlov, A. R. *Ber. Bunsen-Ges. Phys. Chem.* **1996**, *100*, 857.
(18) Scheutjens, J. M. H. M.; Fleer, G. J. *J. Phys. Chem.* **1979**, *83*, 1619.
(19) Scheutjens, J. M. H. M.; Fleer, G. J. *J. Phys. Chem.* **1980**, *84*, 178.
(20) Scheutjens, J. M. H. M.; Fleer, G. J. *Macromolecules* **1985**, *18*, 1882.
(21) Leermakers, F. A. M.; Scheutjens, J. M. H. M. *J. Phys. Chem.* **1989**, *93*, 7417.
(22) Leermakers, F. A. M.; Scheutjens, J. M. H. M. *J. Colloid Interface Sci.* **1990**, *136*, 231.
(23) Van Lent, B.; Scheutjens, J. M. H. M. *Macromolecules* **1989**, *22*, 1931.
(24) Leermakers, F. A. M.; Wijmans, C. M.; Fleer, G. J. *Macromolecules* **1995**, *28*, 3434.
(25) Linse, P. *Macromolecules* **1993**, *26*, 4437.
(26) Hurter, P. N.; Scheutjens, J. M. H. M.; Hatton, T. A. *Macromolecules* **1993**, *26*, 5030.
(27) Linse, P. *Macromolecules* **1994**, *27*, 6404.
(28) Evers, O. A.; Fleer, G. J.; Scheutjens, J. M. H. M.; Luklema, J. *J. Colloid Interface Sci.* **1986**, *111*, 446.
(29) Böhmer, M. R.; Evers, O. A.; Scheutjens, J. M. H. M. *Macromolecules* **1990**, *23*, 2288.
(30) van de Steeg, H. G. M.; Cohen Stuart, M. A.; de Keizer, A.; Bijsterbosch, B. *Langmuir* **1992**, *8*, 2538.
(31) Shubin, V.; Linse, P. *J. Phys. Chem.* **1995**, *99*, 1285.
(32) Linse, P. *Macromolecules* **1996**, *29*, 326.
(33) Linse, P.; Björling, M. *Macromolecules* **1991**, *24*, 6700.
(34) Israels, R.; Leermakers, F. A. M.; Fleer, G. J.; Zhulina, E. B. *Macromolecules* **1994**, *27*, 3249.
(35) Borisov, O. V.; Zhulina, E. B.; Birshtein, T. M. *Macromolecules* **1994**, *27*, 4795.
(36) Zhulina, E. B.; Borisov, O.V. *Macromolecules* **1996**, *29*, 2618.
(37) Daoud, M.; Cotton, J. P. *J. Phys.* **1982**, *43*, 531.
(38) Pincus, P. *Macromolecules* **1991**, *24*, 2912. Ross, R.; Pincus, P. *Macromolecules* **1992**, *25*, 1503.
(39) Borisov, O. V.; Birshtein, T. M.; Zhulina, E. B. *J. Phys. II* **1991**, *1*, 521.
(40) Zhulina, E. B.; Borisov, O. V.; Birshtein, T. M. *J. Phys. II* **1992**, *2*, 63.
(41) Borisov, O. V.; Zhulina, E. B. *Eur. Phys. J., B* **1998**, *4*, 205.
(42) Pincus, P. *Macromolecules* **1976**, *9*, 386.
(43) Alexander, S. *J. Phys. (Paris)* **1977**, *38*, 983.
(44) Israelachvili, J. N. *Intermolecular and Surface Forces*; Academic Press: London, 1985.
(45) Oosawa, F. *Polyelectrolytes*; M. Dekker: New York, 1970.
(46) Shusharina, N. P.; Linse, P.; Khokhlov, A. R. Submitted.

MA9917491